ANTIOXIDANTS & REDOX SIGNALING
Volume 24, Number 3, 2016

DOI: 10.1089/ars.2015.6272

ORIGINAL RESEARCH COMMUNICATION

Redox Activation of the Universally Conserved ATPase YchF by Thioredoxin 1

Liya Hannemann,[1] Ida Suppanz,[2,3] Qiaorui Ba,[1,2] Katherine MacInnes,[1] Friedel Drepper,[2,3] Bettina Warscheid,[2,3] and Hans-Georg Koch[1]

Abstract

Aims: YchF/Ola1 are unconventional members of the universally conserved GTPase family because they preferentially hydrolyze ATP rather than GTP. These ATPases have been associated with various cellular processes and pathologies, including DNA repair, tumorigenesis, and apoptosis. In particular, a possible role in regulating the oxidative stress response has been suggested for both bacterial and human YchF/Ola1. In this study, we analyzed how YchF responds to oxidative stress and how it potentially regulates the antioxidant response. ***Results:*** Our data identify a redox-regulated monomer–dimer equilibrium of YchF as a key event in the functional cycle of YchF. Upon oxidative stress, the oxidation of a conserved and surface-exposed cysteine residue promotes YchF dimerization, which is accompanied by inhibition of the ATPase activity. No dimers were observed in a YchF mutant lacking this cysteine. *In vitro*, the YchF dimer is dissociated by thioredoxin 1 (TrxA) and this stimulates the ATPase activity. The physiological significance of the YchF-thioredoxin 1 interaction was demonstrated by *in vivo* cross-linking, which validated this interaction in living cells. This approach also revealed that both the ATPase domain and the helical domain of YchF are in contact with TrxA. ***Innovation:*** YchF/Ola1 are the first redox-regulated members of the universally conserved GTPase family and are inactivated by oxidation of a conserved cysteine residue within the nucleotide-binding motif. ***Conclusion:*** Our data provide novel insights into the regulation of the so far ill-defined YchF/Ola1 family of proteins and stipulate their role as negative regulators of the oxidative stress response. *Antioxid. Redox Signal*. 24, 141–156.

Introduction

P-Loop GTPases are universally conserved molecular switches that cycle between a GDP-bound off state and a GTP-bound on state. The associated conformational changes then determine complex protein interaction networks that regulate essential processes such as protein synthesis, cellular differentiation, or stress response (52, 54). At least 20 GTPase families have been identified based on structural features and eight of these families are universally conserved in eukaryotes, bacteria, and archaea. Within the Obg (*spo0B-associated GTP-binding protein*) family of GTPases, the YchF/Ola1 proteins constitute an unconventional subfamily because they hydrolyze ATP rather than GTP (24, 49). This is due to an altered G4 motif in the nucleotide-binding domain,

Innovation

YchF/Ola1 represent largely uncharacterized ATP-hydrolyzing members of the universally conserved GTPase family. Our data demonstrate that *Escherichia coli* YchF undergoes a redox-dependent dimerization. This inhibits its ATPase activity and prevents the inhibition of the antioxidant response. The monomer–dimer equilibrium of YchF as well as its ATPase activity is regulated by thioredoxin 1, which was identified by site-directed cross-linking as a major contact partner of YchF *in vivo*. Our data reveal a new regulatory mechanism for controlling the oxidative stress response and identify the YchF/Ola1 subfamily of A(G)TPases as first redox-regulated members of the universally conserved GTPase family.

[1]Institut für Biochemie und Molekularbiologie, [2]Faculty of Biology, and [3]BIOSS Centre for Biological Signalling Studies, Albert-Ludwigs-Universität Freiburg, Freiburg, Germany.

which lacks a lysine residue that determines guanosine specificity (24).

The available crystal structures of *Haemophilus influenzae* YchF (47) and its human homologue hOla1 (24), show three distinct domains: the N-terminal domain displays a typical TRAFAC (*translation factor*)-type fold with a six-stranded mostly parallel β-sheet surrounded by α-helices (Fig. 1A). The second domain is characterized by two α-helices, which often serve as recognition motifs for protein and nucleic acid interaction (35). This YchF domain is similar to the coiled-coil domain in transcription elongation factor GreA (45), pointing to possible RNA interaction. The third domain is located at the C-terminus and shows similarity to TGS domains (*ThrRS-GTPases-SpoT*), which are associated with nucleotide-dependent regulatory functions and nucleic acid binding (2).

Despite its universal conservation, the physiological function of YchF/Ola1 is still unknown. Many Obg-like G/ATPases are involved in ribosome biogenesis and ribosome binding has been observed for *Escherichia coli* (6, 49) and *Trypanosoma cruzi* (16) YchF. The exact impact of YchF on ribosome biogenesis or translation is unknown, but yeast Ola1 possibly influences translational fidelity (39). Whether YchF/Ola1 interact with ribosomal proteins or rRNA is unknown, but the cleft formed by the helical domain and the TGS domain would be wide enough to accommodate nucleic acids (Fig. 1A). A possible role in DNA repair was also postulated because human hOla1 is downregulated upon DNA damage and upregulated in many tumors (46). This was validated by the observation that hOla1 interacts with BRCA1 (*breast cancer-associated gene* 1) at the centrosome and that depletion of hOla1 induced centrosome fragmentation (29). Other functions of Ola1/YchF include a possible role in iron uptake in pathogens (8, 15) and salinity stress in plants (9, 10).

The postulated functions of YchF/Ola1 in different species are difficult to reconcile with a single mode of action. However, in both *E. coli* and humans, overexpression of YchF/Ola1 resulted in H_2O_2 hypersensitivity (53, 56), suggesting a role of YchF/Ola1 in oxidative stress response. This is so far the only predicted function of YchF/Ola1 that appears to be evolutionarily conserved from bacteria to humans. In *E. coli*, YchF was shown to interact with catalase KatG, the major H_2O_2-detoxifying enzyme, and overexpression of YchF decreased catalase activity in *E. coli* cell extracts (53). YchF/Ola1 probably act *via* a transcription- and translation-independent mechanism (56) because overexpression of YchF in *E. coli* had no significant influence on the OxyR-controlled expression of KatG (53). OxyR is a LysR-like transcription factor, which serves as master regulator of the H_2O_2 response in *E. coli* (11). OxyR is activated by H_2O_2, resulting in increased expression of at least 30 proteins that either detoxify H_2O_2 or protect macromolecules against oxidative damage (19). A few genes are also repressed by oxidized OxyR; this includes *oxyR* itself and, intriguingly, *ychF* (19, 53). This demonstrates that YchF is part of the *E. coli* OxyR regulon and probably acts as a negative regulator of the oxidative stress response. In addition, YchF appears to be regulated by complex post-translational modifications, including dephosphorylation of serine 16 (28) and so far unknown modifications, which are required for full ATPase activity in response to H_2O_2 (53).

In the current study, we have analyzed YchF in the model organism *E. coli*. Based on our data, we propose a model for the redox regulation of YchF and its inhibitory effect on the antioxidant response.

Results

YchF forms redox-sensitive dimers

The activity of *E. coli* YchF is regulated by an H_2O_2-dependent dephosphorylation and additional, so far unknown, stress-dependent modifications (53). Redox-sensitive pathways are commonly regulated by either thiol modifications (3) or histidine oxidation (26). *E. coli* YchF contains six cysteine residues, which are highly conserved within enterobacteria and also weakly in other YchF/Ola1 homologues (Fig. 1B). In the structural model of *E. coli* YchF, which was generated using the *H. influenzae* YchF structure (85% sequence identity to *E. coli* YchF), the six cysteine residues are surface exposed (Fig. 1A), making them suitable for regulation *via* thiol oxidation.

To analyze this, YchF was purified from *E. coli* and separated by sodium dodecyl sulfate–polyacrylamide gel electrophoresis (SDS-PAGE) under reducing conditions (+25 m*M* DTT). Western blotting using α-YchF antibodies detected YchF as a strong band at $\sim$40 kDa. In addition, a weak band at $\sim$90 kDa was also detected, which could reflect a YchF dimer (Fig. 2A). Under nonreducing conditions (–DTT), the putative YchF dimer at $\sim$90 kDa was much stronger and less of the monomer was detected (Fig. 2A). In addition, two weaker bands (*) of $\sim$50 kDa and 100 kDa were detected. The band migrating at 90 kDa could, in principle, also correspond to a complex between YchF and additional proteins. To exclude this possibility, the 90 kDa band was cut out of the gel and separated on SDS-PAGE under reducing conditions. Coomassie staining revealed a single band at $\sim$40 kDa (Fig. 2B), demonstrating that the 90 kDa band indeed corresponded to the YchF dimer.

Dimerization of purified YchF could be an artifact of the *in vitro* conditions and we therefore analyzed dimerization in cell extracts of *E. coli* cells expressing YchF under an arabinose-inducible promoter. Western blotting identified the YchF monomer and dimer in these crude cell extracts (Fig. 2C), demonstrating that dimerization is not only observed with purified proteins. We also tried to detect YchF and its dimeric form in wild-type *E. coli* cells, but the low cellular concentration of YchF and the sensitivity of our antibody did not allow for an unambiguous detection of the dimer in whole cells.

The dithiothreitol (DTT)-sensitive YchF dimerization supports the involvement of cysteine residues in dimerization and this was further analyzed by testing their surface accessibility using the thiol-modifying agent, methoxypolyethylene glycol maleimide (PEG-Mal). PEG-Mal binding to cysteines induces a mass shift that can be monitored by SDS-PAGE (7). When YchF was reduced by tris(2-carboxyethyl)phosphine (TCEP), incubated with PEG-Mal, and subsequently analyzed by SDS-PAGE under reducing conditions, we observed seven prominent bands of increasing mass (Fig. 2D). As a control, we constructed and purified a cysteine-free YchF mutant. The Cys-free YchF did not show any mass shift upon PEG-Mal incubation (Fig. 2D). These data indicate that all six cysteine residues are accessible to PEG-Mal modification and thus are surface exposed as predicted from the homology model (Fig. 1A).

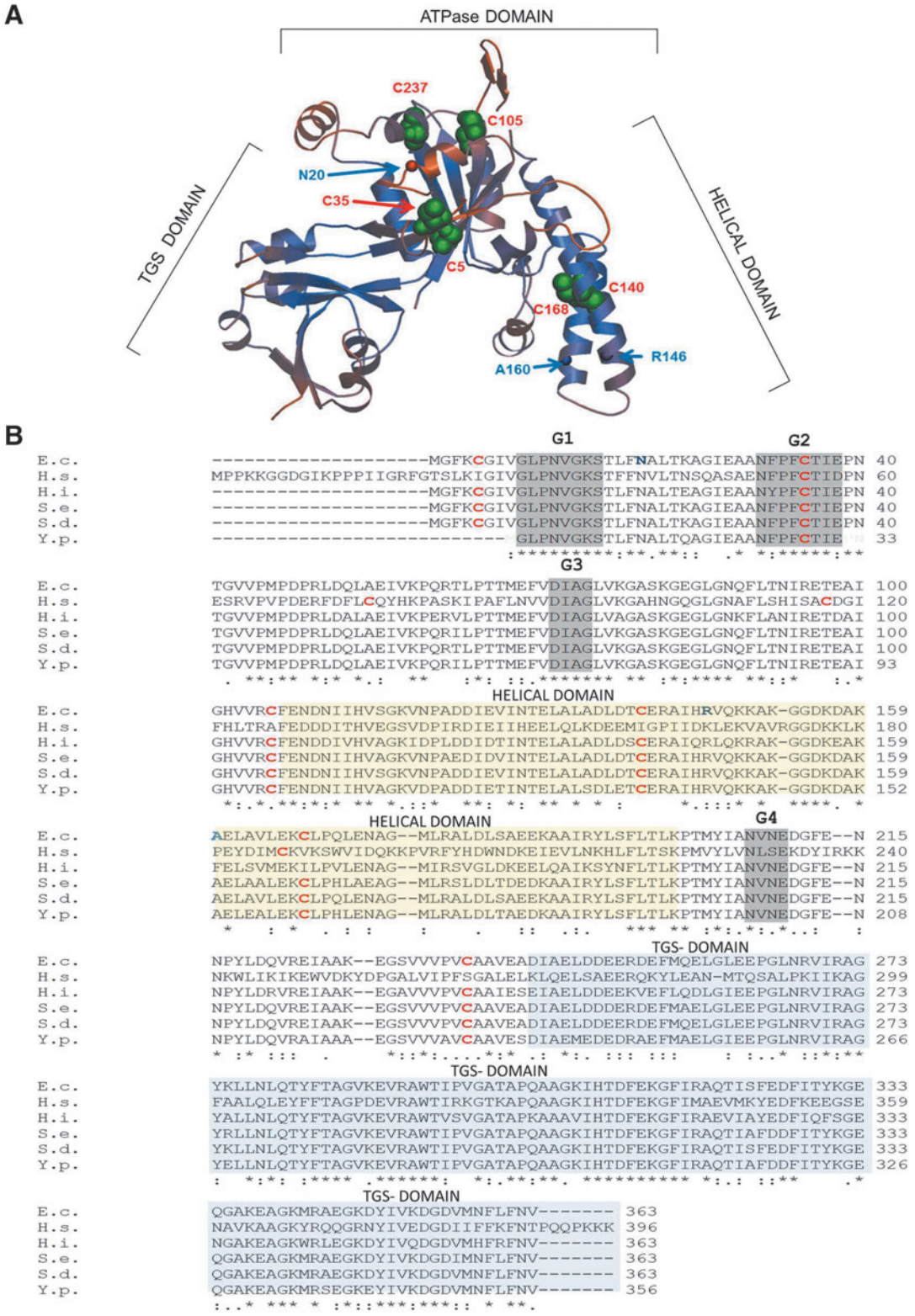

FIG. 1. Position and sequence conservation of cysteine residues in YchF/Ola1. **(A)** The crystal structure of the YchF homologue of *Haemophilus influenzae (1JAL)* was used to model the probable position of the six cysteine residues in *Escherichia coli* YchF using the Swiss Model (http://swissmodel.expasy.org/interactive/kFyFA3/models). Cysteine residues are labeled with *green* spheres and the amino acid position based on the *E. coli* numbering is indicated in *red*. In addition, the residues where the UV-induced cross-linker pBpa was incorporated are indicated by *circles* and the amino acid position based on the *E. coli* numbering is indicated in *blue*. **(B)** A sequence alignment of YchF homologues from different enterobacteria was generated by using the Clustal 2.0 software and compared with the *H. influenzae* YchF and *Homo sapiens* Ola1 sequence. Cysteine residues are shown in *red* and bold and the positions where pBpa was incorporated in the *E. coli* YchF are shown in *blue* and bold. The G1-G4 motifs of the nucleotide-binding site are *boxed* in *gray*, the helical domain is *boxed* in *yellow*, and the TGS domain in *blue*. *E.c.*, *Escherichia coli*; *H.s., Homo sapiens*; *H.i., Haemophilus influenzae*; *S.e., Salmonella enterica*; *Y.p., Yersinia pestis; S.d., Shigella dysentericae*. To see this illustration in color, the reader is referred to the web version of this article at www.liebertpub.com/ars

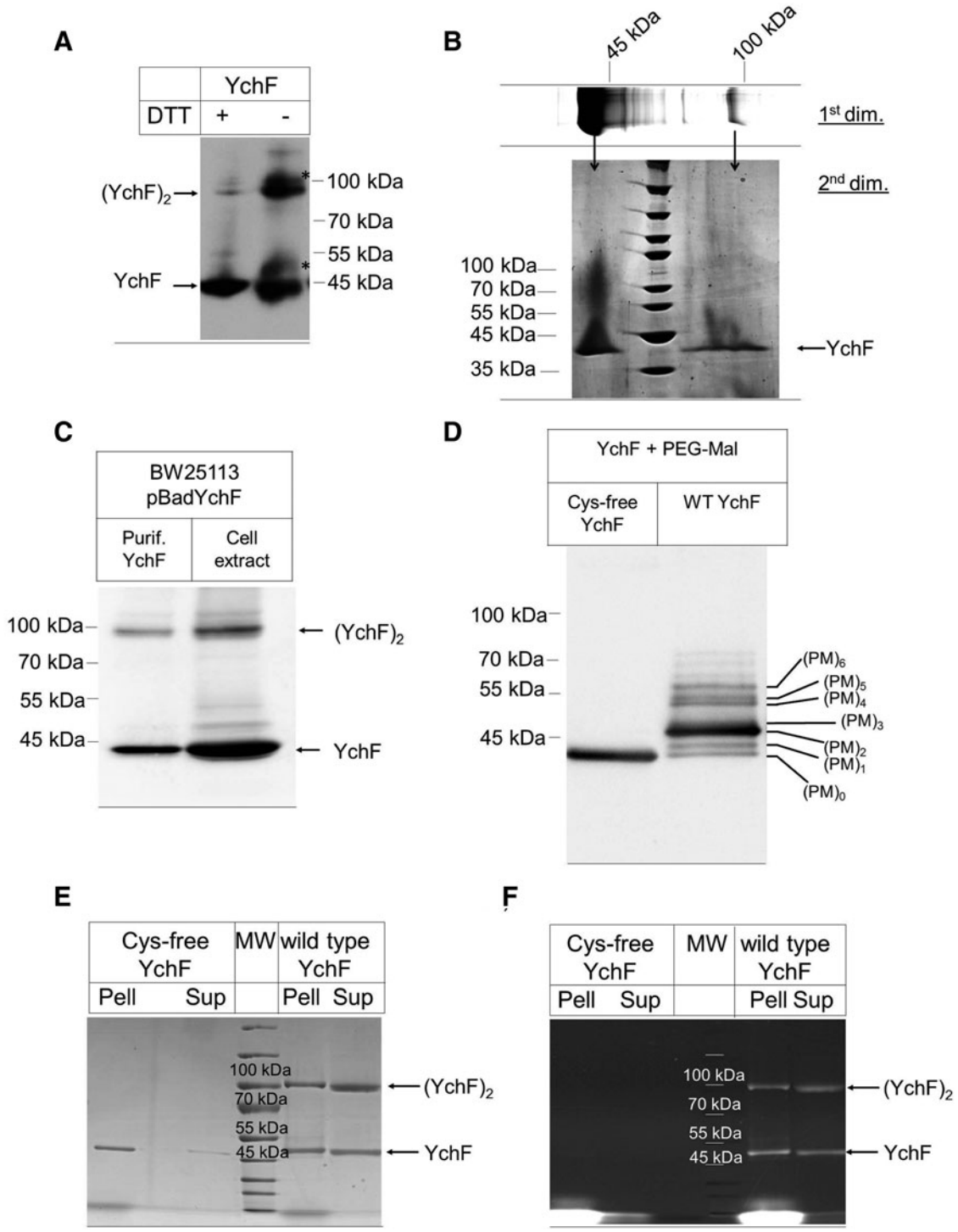

FIG. 2. YchF forms redox- and cysteine-dependent physiological dimers. (A) Purified YchF was denatured at 37°C for 15 min at either reducing (+25 m*M* DTT) or nonreducing conditions (–DTT) and after sodium dodecyl sulfate–polyacrylamide gel electrophoresis (SDS-PAGE) and Western transfer probed with α-YchF antibodies. Two weaker bands were also recognized by α-YchF antibodies (*) in the absence of DTT. **(B)** Purified YchF was separated on SDS-PAGE under nonreducing conditions as in A (1st dim.), and after Coomassie staining, the YchF monomer and dimer bands were excised out of the gel and separated on a second dimension SDS-PAGE (2nd dim.) under reducing conditions. **(C)** Purified YchF and lysozyme-lysed *E. coli* cells expressing YchF were separated under nonreducing conditions on SDS-PAGE and YchF was detected after Western transfer with α-YchF antibodies. **(D)** Purified wild-type YchF (wt YchF) and a cysteine-free derivative (Cys-free YchF) were reduced and incubated with the thiol-modifying agent, PEG-Mal, and subsequently separated by SDS-PAGE. After Western transfer, the membrane was probed with α-YchF antibodies. $(PM)_{0–6}$ reflect the number of labeled cysteines. **(E, F)** Purified Cys-free and wild-type YchF were incubated with the fluorescent thiol-modifying agent fluorescein-5-maleimide. Subsequently, pellet (Pell) and supernatant (Sup) fractions were prepared and samples separated by SDS-PAGE under nonreducing conditions, followed by Coomassie staining **(E)** or in-gel fluorescence analysis **(F)**.

The contribution of the cysteine residues to YchF dimerization was further analyzed by comparing wild-type YchF and the Cys-free YchF mutant by SDS-PAGE under nonreducing conditions. Cys-free YchF showed a tendency to aggregate and purified proteins were therefore subjected to a centrifugation step before SDS-PAGE. For wild-type YchF, we observed both monomer and dimer by Coomassie staining (Fig. 2E). Both forms were almost equally distributed between the supernatant and pellet fraction after centrifugation. For the Cys-free mutant, we observed only the monomeric form, but no dimer (Fig. 2E), which demonstrates that YchF dimerization is cysteine dependent. The Cys-free YchF monomer was predominantly recovered from the pellet fraction after centrifugation, indicating that the cysteine residues are important for folding or solubility of YchF. Dimerization was also analyzed by the cysteine-specific fluorescent dye fluorescein-5-maleimide, which stained both monomer and dimer of wild-type YchF, but not the Cys-free mutant (Fig. 2F). This verifies the absence of cysteine residues in the Cys-free YchF derivative and indicates that not all cysteine residues of wild-type YchF are involved in dimerization. Cys-free YchF was purified under denaturing conditions and subsequently refolded. For excluding the possibility that the absence of the dimer observed for the Cys-free YchF is the result of the purification procedure, we also purified wild-type YchF under denaturing conditions and found both the monomeric and dimeric forms (Supplementary Fig. S1; Supplementary Data are available online at www.liebertpub.com/ars).

The conserved cysteine residue 35 is required for YchF dimerization

For identifying the cysteine residues involved in YchF dimerization, purified YchF was treated with iodoacetamide for blocking free cysteine residues and separated by SDS-PAGE. After colloidal Coomassie staining, the monomer and dimer bands were excised and analyzed by high-resolution mass spectrometry (MS). This approach identified two uniquely cysteine-linked peptides (Table 1 and Fig. 3). In the YchF monomer, peptides containing Cys5 and Cys35 formed a prominent intramolecular disulfide bridge, which was virtually absent in the YchF dimer (Fig. 3A). Instead, Cys35-Cys35-linked peptides were present in the dimer and not in the monomer (Fig. 3B, C). This demonstrates that YchF dimerizes *via* disulfide bridge formation between the Cys35 residues of each monomer, whereas in the monomeric YchF, Cys5 forms an intramolecular disulfide bond to Cys35.

The involvement of Cys35 in YchF dimerization was further verified by analyzing dimer formation in a YchF mutant that contained a cysteine 35-to-serine replacement. In this mutant, almost no YchF dimer was detectable by Coomassie staining or Western blotting (Fig. 3D, E). This confirms that Cys35 is essential for dimer formation. For wild-type YchF and the YchF(C35S) mutant, an additional band at $\sim$50 kDa was detected, suggesting a further Cys35-independent form of YchF. Using MS, we confirmed that YchF is the main component (99.5%) in this band. As minor contamination (0.5%), we only detected 3-dehydroquinate synthase (AroB), which has a molecular mass of 39 kDa and is probably copurifying with YchF. Thus, further analysis is needed to reveal the identity of this Cys35-independent 50-kDa YchF form.

Intriguingly, among the cysteine residues present in different YchF/Ola1 species, Cys35 shows the highest conservation (Fig. 1B). This may indicate that Cys35-linked dimer formation is a general feature of the YchF/Ola1 protein family.

YchF displays redox-activated ATPase activity

To determine the physiological significance of the redox-dependent dimerization, we monitored the ATPase activity of YchF. We first measured the ATPase activity of purified wild-type YchF under reducing (+DTT) and oxidizing conditions (+tetrathionate). The addition of DTT stimulated the ATPase activity of YchF about two-fold, while the addition of tetrathionate significantly reduced the ATPase activity (Fig. 4A).

We then compared the ATPase activity of wild-type YchF with the activity of the YchF(C35S) mutant and the Cys-free YchF. In both the C35S and the Cys-free mutant, we detected an approximately two-fold higher ATPase activity than in the wild type. The addition of DTT had no significant effect on the Cys-free or the C35S YchF mutants (Fig. 4B). In summary, these data demonstrate that the ATPase activity of YchF is determined by its redox-sensitive dimerization. The YchF dimer exhibits only low activity, but the dissociation into the monomer strongly stimulates its ATPase activity.

The overexpression of YchF/Ola1 in *E. coli* or humans increases the sensitivity toward oxidative stress (53, 56). This phenotype depends on the ATPase activity of YchF (53) and we therefore reasoned that expressing the YchF(C35S) mutant should result in enhanced oxidative stress sensitivity,

Table 1. Disulfide-Linked Peptides of YchF Determined by Liquid Chromatography–Tandem Mass Spectrometry

Peptide A sequence	*Peptide B sequence*	*Mass (Mr)/Da*	*Charge state*	*Identified in*	*Area*[a] *dimer*	*Area*[a] *monomer*
C^{5}GIVGLPNVGK	AGIEAANFPF**C**^{35}TIEPNTGVVPM*PDPR	3811.8703	3,4	Monomer	1.5E7	3.9E8
AGIEAANFPF**C**^{35} TIEPNTGVVPM*PDPR	AGIEAANFPF**C**^{35}TIEPNTGVVPM*PDPR	5514.6123	4	Dimer	1.5E8	5.9E6
AGIEAANFPF**C**^{35} TIEPNTGVVPMPDPR	AGIEAANFPF**C**^{35}TIEPNTGVVPM*PDPR	5498.6171	4	Dimer	4.6E7	n. d.

Monomer and dimer bands were excised from the polyacrylamide gel and subjected to in-gel digestion using trypsin, followed by LC-MS/MS analysis. For the identification of disulfide-linked peptides, mass spectrometric data were analyzed using the xQuest/xProphet software suite. Quantitative data analysis was performed with the Skyline software.

[a]chromatographic peak area summed for molecular ion MS1 isotope peaks.

M*, oxidized methionine; n.d., not detected.

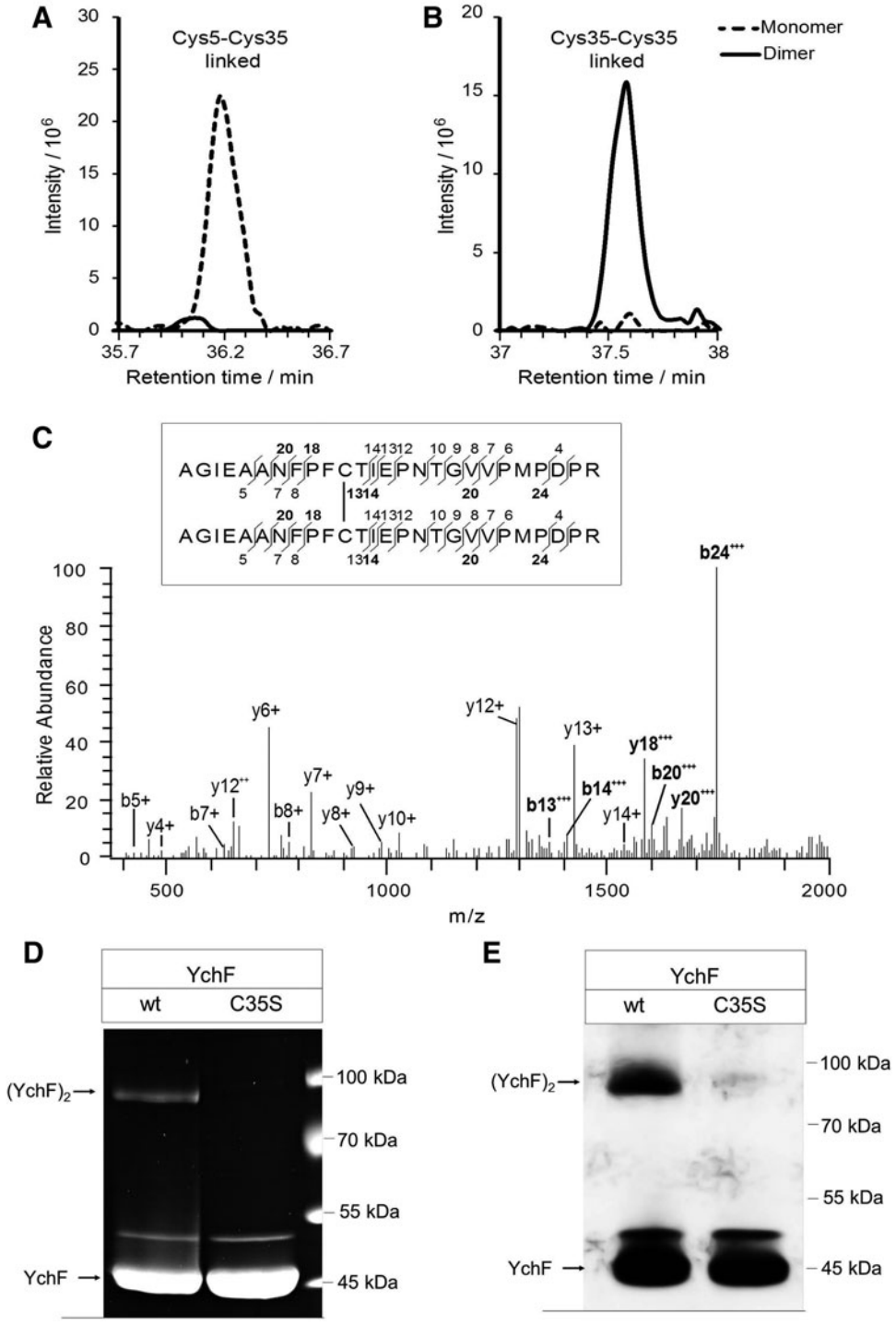

FIG. 3. Identification and quantification of disulfide-linked peptides in YchF monomer and dimer. **(A)** Extracted ion chromatograms of the Cys5-Cys35-linked peptides, CGIVGLPNVGK and AGIEAANFPFCTIEPNTGVVPM*PDPR (precursor *m/z* 953.9757, charge +4), determined by liquid chromatography–mass spectrometry analyses of the monomer (*dashed line*) and dimer band (*solid line*). **(B)** Equivalent to A, but for the Cys35-Cys35-linked peptide AGIEAANFPFCTIEPNTGVVPM*PDPR (precursor *m/z* 1379.6581, charge +4). **(C)** Fragment spectrum of the Cys35-Cys35 disulfide-linked peptide AGIEAANFPFCTIEPNTGVVPM*PDPR. b- and y-type fragment ions are annotated in the mass spectrum and in the sequence (*inset*). Fragments containing the disulfide bridge are shown in bold. **(D)** Wild-type YchF and YchF containing a single cysteine-to-serine replacement at position 35 (YchFC35S) were purified and separated by SDS-PAGE under nonreducing conditions. Proteins were subsequently stained with Coomassie. **(E)** As in **D**, but samples were probed with α-YchF antibodies after Western blotting. M*, oxidized methionine.

which was induced by the thiol-modifying agent, diamide. Diamide induces reversible non-native disulfide bonds in cytoplasmic proteins (19), thereby reducing the free thiol concentration. Diamide sensitivity was analyzed by agar diffusion assays (Fig. 4C) and by spotting serially diluted cells on diamide-containing plates (Fig. 4D). Both assays demonstrated increased sensitivity of the YchF(C35S)-expressing Δ*ychF* strain compared with the Δ*ychF* strain expressing wild-type YchF or the plasmid-free Δ*ychF* strain (Fig. 4C, D). Expressing the ATPase-deficient YchF(P11A/N12A) derivative, which shows reduced ATPase activity (53), had only a minor effect on diamide sensitivity (Fig. 4C). These data indicate that the high ATPase activity of the YchF(C35S) mutant inhibits the ability of *E. coli* to cope with oxidative stress.

YchF interacts with thioredoxin 1 in vivo

The redox-sensitive monomer–dimer transition of YchF and its effect on the ATPase activity raised the question about

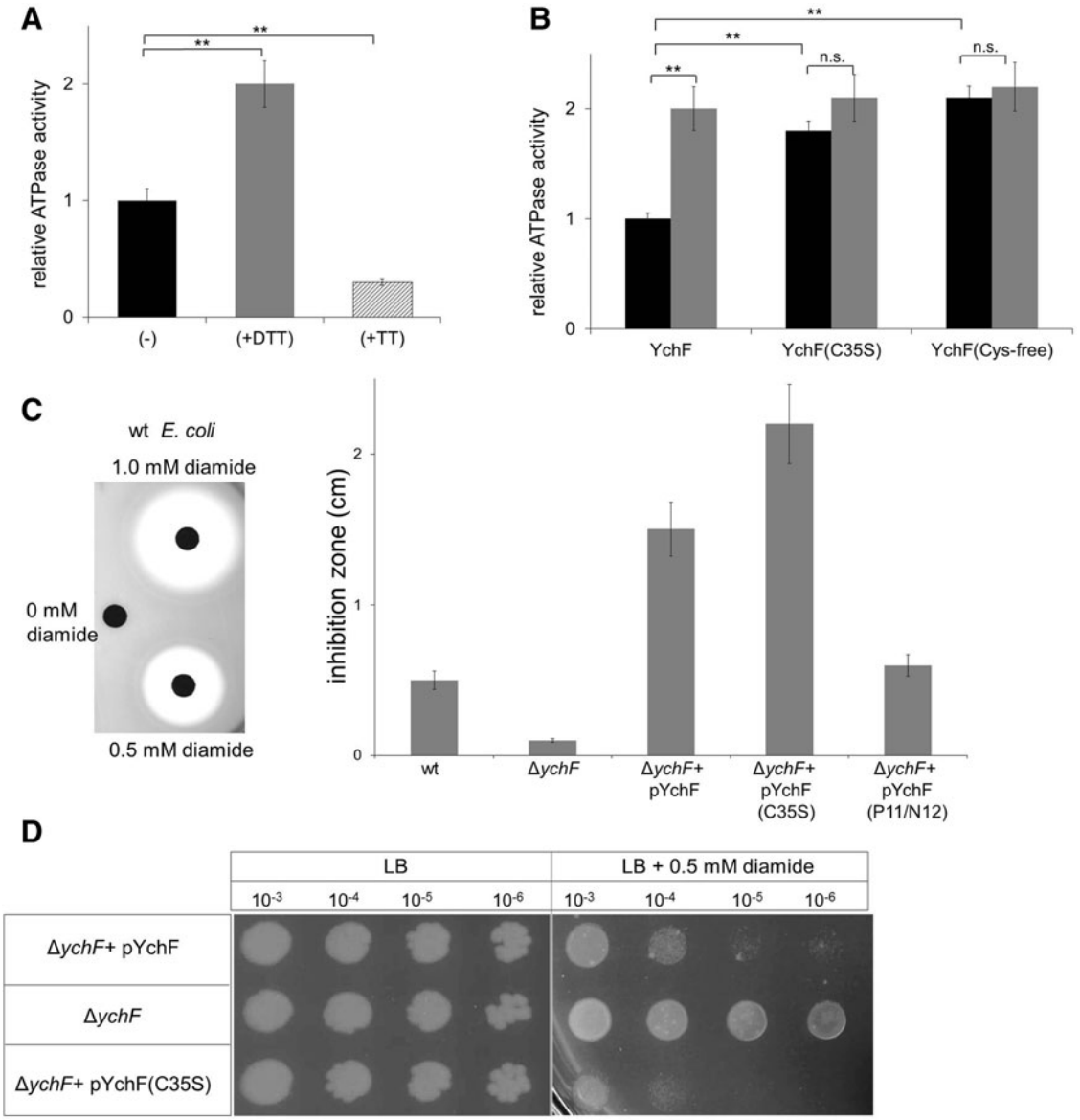

FIG. 4. Dimerization of YchF inhibits its ATPase activity (A) The ATPase activity of purified wild-type YchF (*black bar*) was determined by measuring phosphate release of γ-^{33}P-labeled ATP. When indicated, YchF was preincubated with either 10 m*M* DTT (*gray bar*) or 10 m*M* tetrathionate (TT) (*hatched bar*) for 5 min at room temperature before measuring the activity. A relative YchF activity of 1 corresponds to $\sim$0.35 nmol ATP/(min $\times$ mg protein). The relative ATPase activities shown are the mean $\pm$ SD ($n > 3$). $^{**}p < 0.01$. **(B)** The ATPase activities of wild-type YchF, the YchF(C35S) mutant, and of the cysteine-free YchF mutant were determined without (*black bars*) or after preincubation with 10 m*M* DTT (*gray bars*). A relative YchF activity of 1 corresponds to $\sim$0.35 nmol ATP/(min $\times$ mg protein). The relative ATPase activities shown are the mean $\pm$ SD ($n = 3$). $^{**}p < 0.01$; n.s. not significant. **(C)** *E. coli* strains were adjusted to an optical density of 0.5, mixed with *Top* agar, and poured on LB Plates. Filter discs were soaked with different diamide concentrations and placed on these plates. Inhibition zones were quantified after $\sim$5 h of growth and the results for wild-type *E. coli* are shown (*left panel*). Quantification of two independent experiments in the presence of 0.5 m*M* diamide (*right panel*). pYchF(P11/N12) corresponds to an ATPase-deficient YchF derivative. **(D)** The indicated *E. coli* strains were grown overnight on liquid LB medium without antibiotics and adjusted to an optical density of 1.0 before serial dilution. Dilutions were then spotted onto LB plates or LB plates containing 0.5 m*M* diamide. Plates were incubated at 37°C and analyzed after $\sim$12 h of growth.

the physiological redox partner proteins of YchF. This was addressed by using a site-directed *in vivo* photo-cross-linking approach with para-benzoyl-L-phenylalanine (pBpa). pBpa can be incorporated specifically at amber stop codon positions in the presence of a plasmid-borne orthogonal aminoacyl-tRNA synthetase/$tRNA_{CUA}$ pair (37). pBpa was first incorporated into position 20 of YchF. Position 20 is located between cysteine residues, Cys5 and Cys35, and had been cross-linked to catalase KatG (53). *E. coli* cells expressing pBad-YchF(N20pBpa) were UV exposed to induce the cross-link reaction *in vivo* and YchF and its cross-linked partner proteins were then purified. As a control, we analyzed

samples without UV exposure and samples from cells expressing pBad-YchF without pBpa. Following SDS-PAGE and MS analysis of cross-linked samples and the respective controls, we analyzed the data specifically for cross-links between YchF and proteins that are either associated with the oxidative stress response or involved in maintaining redox homeostasis. In support of previous data (53), we found the *E. coli* catalases, KatG and KatE, as well as the large subunit of the alkyl hydroperoxide reductase AhpF cross-linked to YchF at position 20 (Table 2). KatG, KatE, and AhpF were also identified in the purified YchF sample without UV exposure (Table 2), supporting the previously observed copurification of these proteins together with YchF. When searching the MS data for potential YchF cross-links to proteins controlling redox homeostasis, we found strong cross-links to thioredoxin 1 (TrxA) and weaker cross-links to thioredoxin 2 (TrxC), peroxiredoxin, and glutaredoxin-4 (Table 2).

The strong cross-link between YchF and TrxA was further verified by immune detection. When YchF was purified from UV-exposed *E. coli* pBad-YchF(N20pBpa) cells, we observed a strong UV-dependent band at ~50 kDa, which was recognized by α-TrxA antibodies (Fig. 5A). This band was absent when pBad-YchF(N20pBpa) was expressed in a Δ*trxA* knockout strain. These data demonstrate that YchF interacts with TrxA *in vivo*. We also noticed that TrxA copurified with YchF because it was detected as an ~10 kDa band in the purified YchF sample (Fig. 5A). Upon UV exposure, the copurifying TrxA amount became significantly weaker, presumably because most of TrxA was cross-linked to YchF (Fig. 5A). To analyze the contribution of the cysteine residues of YchF to the TrxA interaction, we reduced the concentration of available thiol groups by treating the cells before cross-linking with a low concentration of diamide. At concentrations below 100 μM, diamide does not induce the OxyR response (58) and, in agreement with this, the diamide-treated sample did not show significantly changed YchF or TrxA levels (Fig. 5B). However, upon diamide treatment, we observed a significant reduction in the YchF-TrxA cross-linking efficiency (Fig. 5C). We also analyzed the cross-link between YchF and peroxiredoxin and found reduced amounts of the cross-linked product upon diamide treatment (Fig. 5D). Thus, decreasing the number of available thiol groups impairs the interaction of YchF with TrxA and peroxiredoxin, which suggests that the cysteine residues of YchF are important for these interactions.

The specificity of the YchF-TrxA interaction was further analyzed by incorporating pBpa into positions 146 and 160 of YchF. These residues are close to Cys140 and Cys168 and located within a predicted coiled-coil structure of YchF. Western blotting showed YchF-TrxA cross-links for both positions (Fig. 6), which were confirmed by MS. However, the cross-linked products from positions 146 and 160 appeared weaker than the cross-link from the N20 residue. Furthermore, both cross-linked products migrated as a double band; a weaker band migrating at ~50 kDa, and a stronger band migrating at ~55 kDa. Position-dependent mobility of pBpa cross-linked products on SDS-PAGE is frequently observed (25, 31, 38) and probably the result of differences in the three-dimensional structures of the cross-linking products. We also noticed less TrxA copurifying with YchF that had pBpa inserted into positions 140 and 160, which could indicate that pBpa insertion at these residues reduces the YchF-TrxA interaction.

In summary, our data show that the N-terminus of YchF and the predicted coiled-coil domain are cross-linked to TrxA. Reducing the concentration of free thiol groups by diamide treatment reduces the YchF-TrxA cross-linking efficiency, suggesting that the YchF-TrxA interaction probably involves mixed disulfides.

Thioredoxin 1 activates the ATPase activity of YchF by dimer dissociation

The physiological significance of the YchF-TrxA interaction was determined by analyzing the ATPase activity of YchF in the presence or absence of TrxA. TrxA was added to purified YchF and the ATPase activity was measured. In the

Table 2. YchF Interacts with Proteins of the Antioxidant Response

	YchF(N20pBpa)				
Protein[a]	*Mol. Mass*[b] *(kDa)*	*Gel Mol. Mass*[c] *(kDa)*	*Rel. Intensity*[d] *(−UV/ +UV)*	*Coverage*[e] *(%)*	*Peptides*[f]
Catalase G (KatG)	80	120	0.6	68	70
Catalase E (KatE)	84	120	0.3	9	6
Alkyl peroxidase subunit F (AhpF)	56	95	0.7	78	56
Thioredoxin 1 (TrxA)	12	55	0.001	78	8
Thioredoxin 2 (TrxC)	16	60	0	8.6	1
Peroxiredoxin (Bcp)	18	86	0	35	4
Glutaredoxin 4	13	55	0	19	2

Cells expressing YchF with the UV-activated cross-linker pBpa at position 20 of YchF were grown on LB medium and one half was UV exposed (+UV), while the other half served as control (−UV). YchF was purified from both samples and separated by sodium dodecyl sulfate–polyacrylamide gel electrophoresis. Equal gel slices were cut out from both lanes, followed by in-gel digestion using trypsin and mass spectrometric analysis. Shown are data obtained for *Escherichia coli* proteins involved in antioxidant response.

[a]Protein identified.
[b]Calculated molecular mass.
[c]Molecular mass of cross-linking product determined by extrapolation.
[d]Relative intensity observed in gel slices from the control lane (−UV) compared with the +UV lane.
[e]Sequence coverage of total sequence by detected peptides.
[f]Number of unique peptides detected.

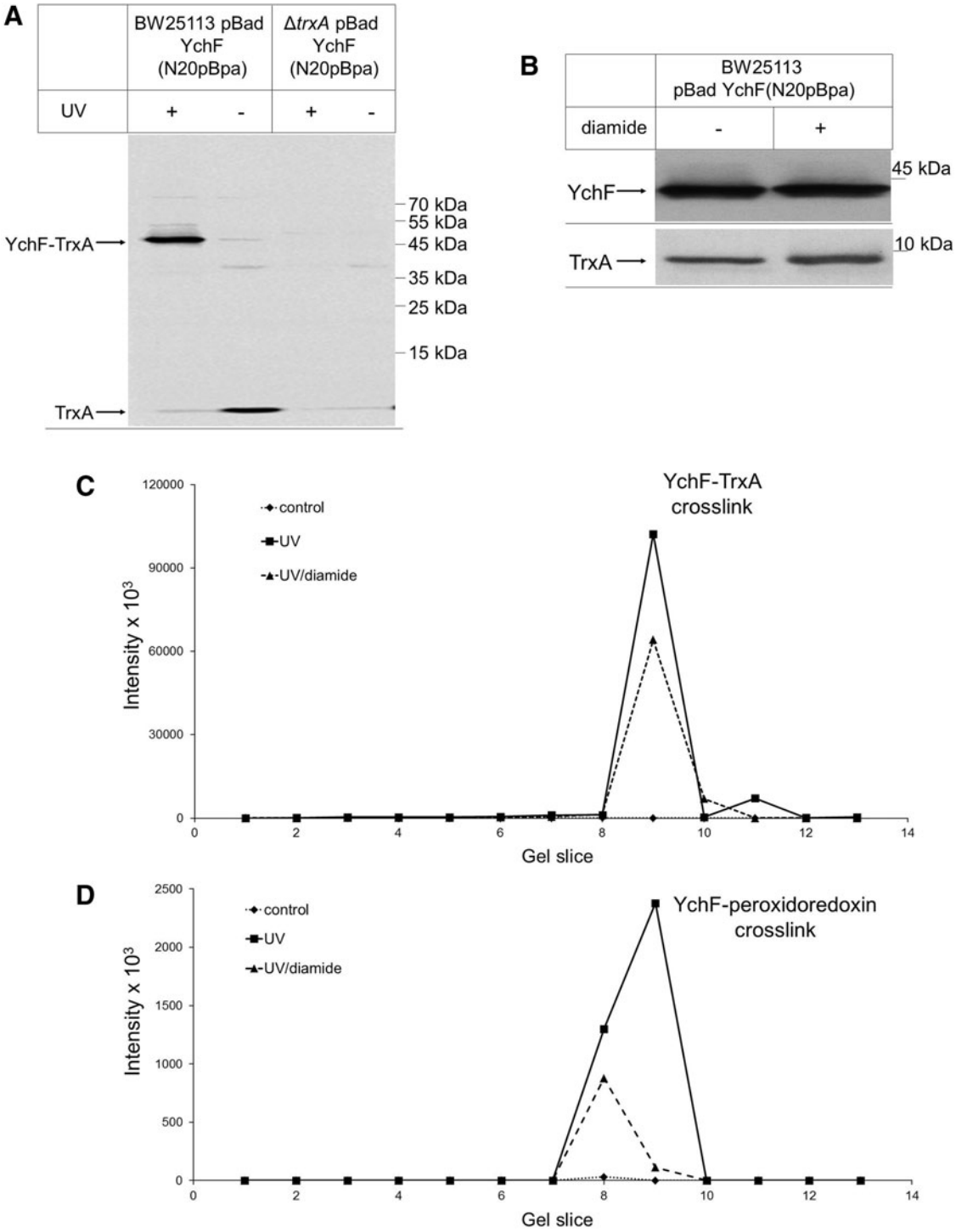

FIG. 5. YchF cross-links to thioredoxin *in vivo*. (A) Wild-type *E. coli* cells or a Δ*trxA E. coli* strain expressing YchF with the UV-dependent cross-linker pBpA incorporated at position N20 were either UV exposed (+) or kept in the dark (−). After cross-linking, YchF was purified, separated by SDS-PAGE, and after Western transfer probed with α-TrxA antibodies. **(B)** Wild-type *E. coli* cells expressing YchF(N20pBpa) were treated with 50 μM diamide and TCA precipitated. The pellet after centrifugation was separated by SDS-PAGE and after Western transfer probed with either α-YchF or with α-TrxA antibodies, **(C, D)** YchF(N20pBpa) cross-linking products were separated by SDS-PAGE, individual gel slices corresponding to the MW range of 130 to 40 kDa were excised, subjected to in-gel digestion using trypsin, and analyzed by mass spectrometry. Data were analyzed for peptides derived from TrxA **(C)** and peroxiredoxin **(D)**. Shown are summed peptide intensities measured in samples obtained without UV exposure (noncross-linked, ◆, *dotted line*), after UV exposure (cross-linked, ■, *solid line*), and after UV exposure of diamide-treated cells (▲, *dashed line*).

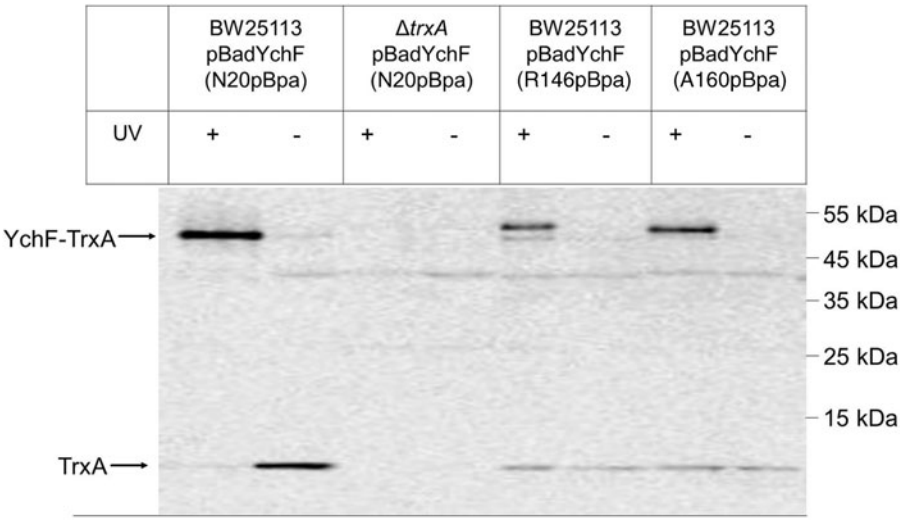

FIG. 6. Thioredoxin interacts with both the N-terminus and the helical domain of YchF *in vivo*. *In vivo* cross-linking was performed as in Fig. 5 with pBpa inserted at position N20, R146, or N160. Samples were subsequently analyzed by Western blotting using α-TrxA antibodies. Cross-linked products of positions, R146 and 160, migrated in two distinct species, which is a common phenomenon of pBpa cross-linking (25, 31, 38) and probably reflects different three-dimensional structures.

presence of equimolar amounts of TrxA, we observed about two-fold stimulation of the YchF ATPase activity, which was comparable with the stimulatory effect of DTT (Fig. 7A). The stepwise increase of the TrxA concentration to a YchF:TrxA ratio of 1:4 did not significantly stimulate the ATPase activity further (Fig. 7A). These data demonstrate that the YchF-TrxA interaction accelerates the ATPase activity of YchF and establish the physiological significance of the YchF-TrxA interaction observed *via in vivo* cross-linking.

We also tested whether TrxA would dissociate the YchF dimer. When purified YchF was separated under nonreducing conditions by SDS-PAGE, we observed both the YchF monomer and dimer by Western blotting (Fig. 7B). However, when YchF was incubated with TrxA before SDS-PAGE and Western blotting, the YchF dimer was almost undetectable. As a control, we added TrxA to YchF without further incubation and separated it directly on SDS-PAGE. Even without additional incubation, TrxA significantly reduced the YchF dimer. Thus, TrxA dissociates the YchF dimer, which concomitantly stimulates the ATPase activity of YchF.

Discussion

The YchF/Ola1 subfamily constitutes one of the most conserved members of the P-Loop GTPase family and is characterized by its unique preference for ATP (24, 52). Sequence comparison between *E. coli* YchF and human hOla1 revealed 45% sequence identity and 62% sequence similarity, but there is so far no clear consensus about the possible role of this protein family. Disclosing cellular targets of YchF/Ola1 is of significant importance because human Ola1 appears to play a major role in pathogenicity and disease development. Ola1 expression is regulated by DNA damage (32, 46) and is upregulated in many human tumors (46). On the other hand, a downregulation of Ola1 is observed in interferon β-treated multiple sclerosis patients (14). Furthermore, cell proliferation and apoptosis seem to be influenced by Ola1 (23). In both bacteria and humans, overexpression of YchF/Ola1 increases the sensitivity toward oxidative stress (53, 56, 57) and an imbalance of the oxidative stress response could potentially provide the link between DNA damage repair (40), the pathogenesis of multiple sclerosis (30), and apoptosis (43).

The YchF/Ola1 mode of action is unknown, but the available data support a role as inhibitor of the oxidative stress response by a transcription- and translation-independent mechanism (53, 56). *E. coli* cells expressing ATPase-deficient YchF derivatives do not display H_2O_2 hypersensitivity (53). This suggests that the ATPase activity of YchF is required for inhibition of the oxidative stress response, probably by regulating the interaction of YchF with proteins such as KatG or the iron scavenger Dps (19, 53). The ATPase activity is subject to a complex regulatory regime (53) and our data now demonstrate that YchF undergoes a reversible redox-sensitive dimerization, which inactivates its ATPase activity. Dimer formation depends on Cys35, which is conserved from *E. coli* to humans and located next to the conserved threonine residue within the G2 motif of the ATPase domain (Fig. 1). This provides the explanation for the ATPase-inhibiting effect of YchF dimerization. The G2 motif serves as the effector region of GTPases, and hydrogen bonds between the threonine residue and the γ-phosphate are required for catalysis and the subsequent conformational changes (54). This so-called loaded spring mechanism is most likely impaired upon disulfide bond formation of the nearby cysteine residue.

TrxA or reducing agents such as DTT dissociate the YchF dimer and activate its full ATPase activity. Thus, the redox-regulated monomer–dimer equilibrium of YchF appears to be a key event in the functional cycle of YchF. Wild-type *E. coli* cells produce $\sim 15\,\mu M$ H_2O_2/s (41), which is too low for significant thiol oxidation (19). Still, we observed YchF dimer formation in *E. coli* cells without H_2O_2 treatment. This could indicate that the active site thiols of YchF are unusually reactive, which has also been observed for OxyR and AhpCF (4). In addition, the detection of YchF in *E. coli* cells by Western blotting required moderate overexpression. Assuming that YchF inhibits the antioxidant response, the endogenous H_2O_2 concentration in YchF-overexpressing cells might actually be higher than in wild-type *E. coli* cells, which would promote the formation and stability of the YchF dimer even in the absence of exogenous H_2O_2. Our current model suggests that under native conditions, YchF exists predominantly as a monomer due to the reducing conditions in the bacterial cytosol. This would allow for the full ATPase activity, which is required for inactivation of antioxidant

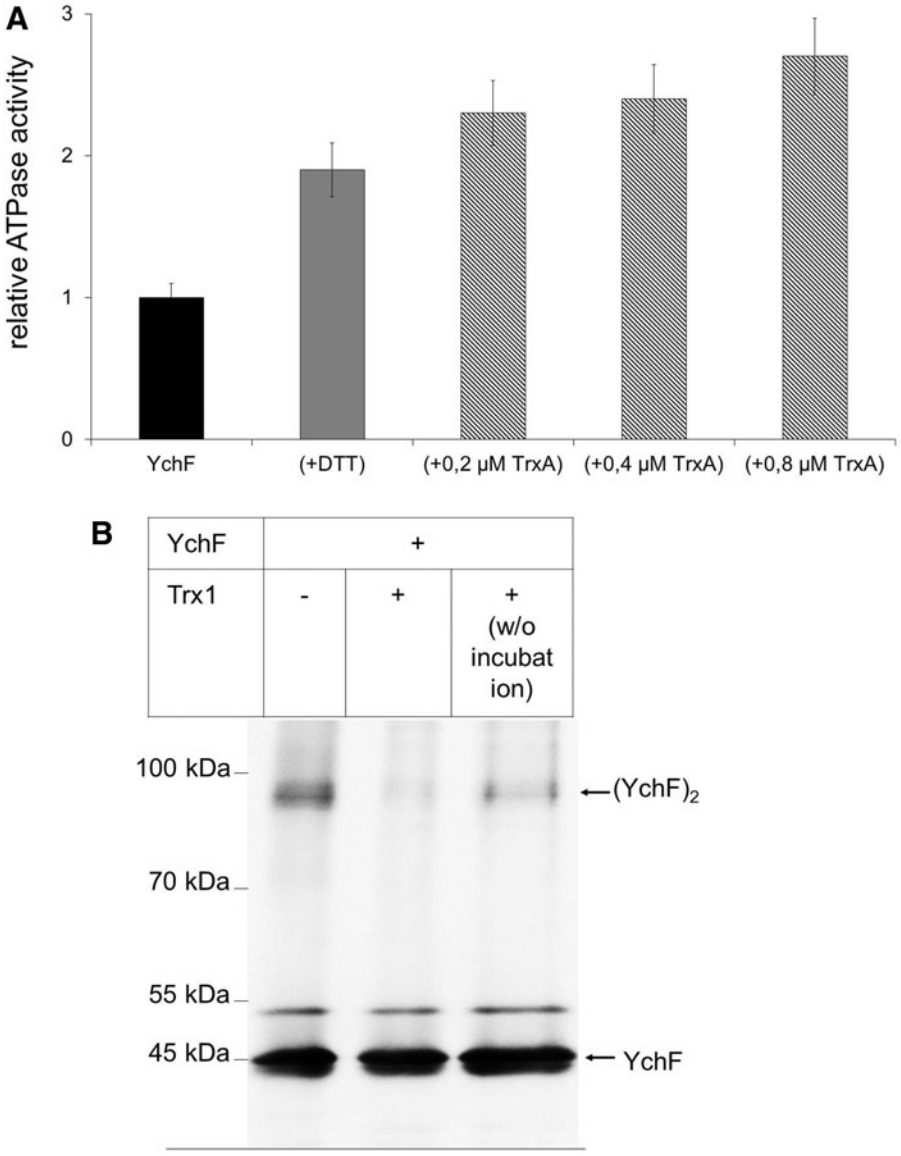

FIG. 7. Thioredoxin increases the ATPase activity of YchF and reduces the YchF dimer. (A) Purified YchF (0.2 μM) was incubated with either DTT (10 mM) (*gray bar*) or increasing TrxA concentrations (*hatched bars*) and the ATPase activity was measured as in Fig. 4. The activity of wild-type YchF was set to one and corresponds to 0.35 nmol ATP/(min × mg protein). The values observed were corrected for the background ATP hydrolysis detected in the purified TrxA sample. **(B)** Purified YchF was incubated for 30 min at 37°C in the presence or absence of purified TrxA in a 1:1 molar ratio. As a control, TrxA was added to YchF without further incubation (w/o incubation). Samples were analyzed by SDS-PAGE under nonreducing conditions and probed with α-YchF antibodies after Western transfer.

enzymes. In the presence of oxidative stress, YchF dimerization would prevent ATP hydrolysis and the inhibitory effect of YchF on antioxidant enzymes diminishes (Fig. 8). Redox-dependent dimerization is a well-known effect in biology and has been observed in response to oxidative stress for peroxiredoxins (5), mitofusins (42), or the redox chaperone, Hsp33 (18). Dimer dissociation of peroxiredoxin and Hsp33 is facilitated by the thioredoxin and glutaredoxin systems (18, 27), similar to what we observe for YchF. Intriguingly, our data identified TrxA as the predominant redox partner of YchF. In contrast to TrxC, TrxA in *E. coli* is not under OxyR control (59, 60) and thus not upregulated in the presence of oxidative stress. This probably reduces YchF monomerization under oxidative stress conditions.

In YchF-overexpressing cells, catalase activity is reduced (53) and the interaction of YchF with the three main H_2O_2-detoxifying enzymes, KatG, KatE, AhpCF, in *E. coli* has been demonstrated (Table 2) (53). Still, the exact mechanism of catalase inhibition remains to be identified. YchF could serve as a trap for these enzymes under nonstress conditions, allowing their immediate reactivation upon oxidative stress. This strategy could be part of the adaptive response against oxidative stress that has been observed in both bacteria and eukaryotes (20). The regulation of H_2O_2-degrading enzymes is also important for H_2O_2-dependent signaling processes, which stimulate cell proliferation and migration in eukaryotic cells (51). A role of Ola1/YchF in regulating the endogenous H_2O_2 concentration is supported by several observations. Knockdown of Ola1 has been shown to influence the migration of cancer cells, probably by modulation of the intracellular ROS levels (57). In addition, focal adhesion kinase is downregulated in H_2O_2-treated mesenchymal stem cells (44), but upregulated upon Ola1 knockdown (22), which is expected if Ola1 inhibits H_2O_2-degrading enzymes. The existence of H_2O_2-dependent signaling processes in bacteria has not been clearly demonstrated, but the catalytic mechanism of catalases might be a further reason for their inhibition in the absence of oxidative stress. At low H_2O_2 concentrations, the two-step catalytic cycle of catalases can stall with the heme cofactor in its ferryl intermediate state (36), which

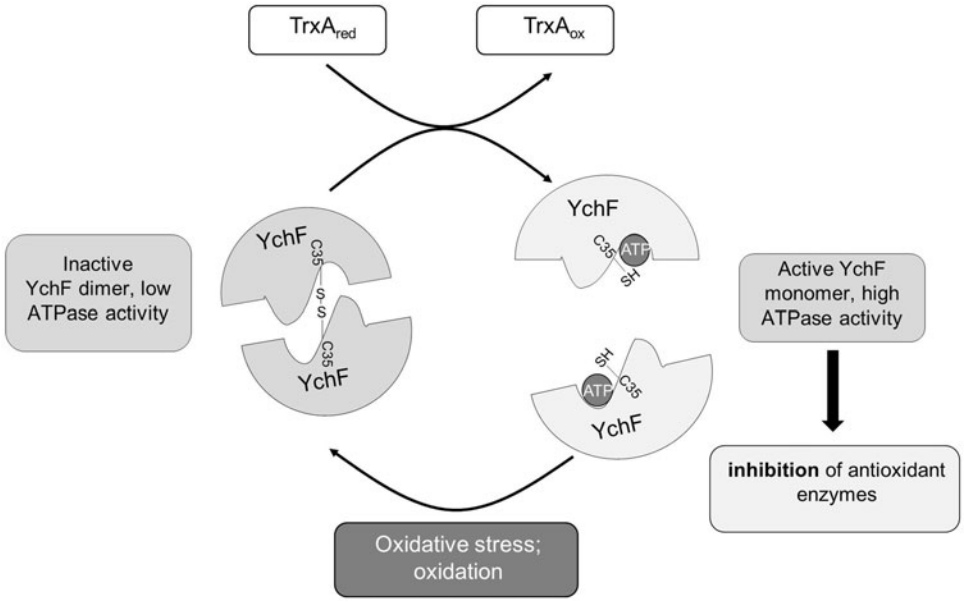

FIG. 8. Model for the redox regulation of YchF, a universally conserved inhibitor of the oxidative stress response. YchF acts as inhibitor of the oxidative stress response in both *E. coli* (53) and *H. sapiens* (56, 57). Oxidative stress regulates YchF expression and activity at both the transcriptional level (53) and the post-translational level. In the absence of oxidative stress, YchF exists primarily as a monomer with high ATPase activity, which is required for the inhibition of antioxidant enzymes. Upon oxidative stress, cysteine residue 35, which is located within the G2 motif of the ATPase domain, is oxidized, leading to YchF dimer formation, which prevents ATP hydrolysis. YchF dimerization upon oxidative stress probably includes an intramolecular disulfide bridge between cysteine 5 and cysteine 35 as an intermediate. Dimerization and concomitant ATPase inhibition alleviate the inhibition of antioxidant enzymes. If oxidative stress eases, YchF dimers are dissociated by the activity of thioredoxin 1 (TrxA).

will then abstract electrons from the surrounding polypeptide and thus function as a damaging oxidant. In addition, catalase peroxidases also efficiently oxidize NAD(P)H, which is linked to superoxide radical formation (19). Thus, the post-translational inhibition of antioxidant enzymes in the absence of oxidative stress is probably important for both unicellular and multicellular organisms.

The interaction between YchF and TrxA probably adds to the multiple effects that are associated with YchF/Ola1 overexpression because this will likely reduce the concentration of thioredoxin available for other cellular processes. In eukaryotic cells, the thioredoxin-interacting protein, Txnip, has been shown to be a key element of cellular redox regulation because it inhibits thioredoxin activity (34). Txnip promotes apoptosis, increases ROS production, and influences metastasis (55), phenotypes which have also been associated with increased Ola1 concentrations (23, 46, 56).

Finally, the involvement of YchF/Ola1 in regulating oxidative stress could also explain why these proteins hydrolyze ATP rather than GTP. Guanine is particularly sensitive to oxidation due to its low redox potential (17), and the product of guanine oxidation, 7,8-dihydro-8-oxoguanine, is routinely determined for monitoring oxidative DNA damage (21). ATP has a significantly higher redox potential compared with GTP (48) and is less sensitive toward oxidation. Furthermore, upon oxidative stress, the ATP level transiently increases, probably due to the inhibition of energy-consuming processes (1). Using ATP rather than GTP could therefore reflect the functional adaptation of the Ola1/YchF subfamily to regulation of the oxidative stress response.

Materials and Methods

Bacterial strains and growth conditions

E. coli strains, BW25113, MRE600, BL21, and BL21(DE3), were used as wild-type strains and were grown in LB medium at 37°C; 25 μg/ml kanamycin was added for the growth of JW1194 (Δ*ychF*) and MY1013 (Δ*trxA*); 50 μg/ml ampicillin was added for strains carrying pBad-*ychF* or its derivatives; and 35 μg/ml chloramphenicol for strains carrying pSup-BpaRS-6TRN (37). Plasmid construction and mutagenesis are described in Supplementary Data. Spot assays and inhibition assays in the presence of diamide were performed as described for H_2O_2 (53).

Protein purification and ATPase assay

To purify N-terminally His-tagged thioredoxin 1, BL21-carrying pET19b-*trxA* was grown to an optical density (OD) of 0.5, and then induced by 1 m*M* IPTG. After 3 h, cells were harvested, resuspended in EPTX buffer (25 m*M* HEPES KOH, pH 7.5, 1 *M* NH_4-acetate, 0.4 m*M* Mg-acetate), and stored at −20°C. After thawing, Complete protease inhibitor mixture (Roche) and phenylmethylsulfonyl fluoride (PMSF, final concentration 0.5 m*M*) were added. Cells were lysed thrice by a French pressure cell (Thermo Scientific). Cell debris was removed by centrifugation (30 min, 15,500 rpm, Sorvall SS-34 rotor). The supernatant was centrifuged for 1 h at 50,000 rpm (Beckmann Ti50 rotor). The supernatant was mixed with EPTX (+5 m*M* imidazole)-equilibrated Talon beads (Clontech) and incubated at 4°C for 2 h. The Talon

beads were washed five times with 3 ml 5 m*M* imidazole in EPTX buffer and proteins were eluted with an imidazole gradient (100–300 m*M*) in EPTX buffer. Eluted proteins were buffer exchanged to 1× HT buffer (50 m*M* Hepes-KOH, pH 7.6; 100 m*M* K-acetate, 10 m*M* Mg-acetate) using PD10 columns (GE Healthcare).

Purification of YchF carrying a C-terminal His-tag followed the same protocol, but cells were induced with 0.001% arabinose. Cysteine-free YchF was purified from inclusion bodies after the first centrifugation step. The pellet was resuspended in 6 *M* urea in EPTX buffer at 4°C for 5 h. After centrifugation (15,500 rpm, 30 min, Sorvall SS-34 rotor) the supernatant was incubated with EPTX-equilibrated Talon beads and further purified as described above. ATPase activity of YchF was determined by measuring hydrolysis of γ-^{33}P-labeled ATP (53).

Cell disruption with lysozyme

E. coli cells were grown to an OD of 0.5 and YchF expression was induced by 0.001% arabinose. Two hours after induction, cells were harvested and washed twice with Tris-HCl (pH 8.0). After centrifugation, the cells were resuspended in Tris-HCl (pH 8.0), 1 m*M* EDTA, 25 m*M* NaCl containing lysozyme (Sigma) (10 mg/ml), Complete protease inhibitor (Roche), and 0.5 m*M* PMSF. The suspension was incubated for 30 min at 37°C. Subsequently, the cells were frozen five times in liquid nitrogen and thawed in water. The suspension was centrifuged (14,000 rpm, 10 min) and the supernatant was loaded onto an SDS-PAGE.

Sodium dodecyl sulfate–polyacrylamide gel electrophoresis

Samples were denatured at 37°C for 10 min. Samples for nonreducing SDS-PAGE were resuspended in DTT-free 4x Laemmli loading buffer (278 m*M* Tris-HCl, pH 6.8, 44.4% glycerol, 4.4% SDS, 0.02% bromophenol blue). Reducing loading buffer contained fresh DTT at a final concentration of 25 m*M*.

For two-dimensional SDS-PAGE, purified YchF was separated by nonreducing SDS-PAGE as the first dimension. The gel was stained with colloidal Coomassie and the YchF monomer and dimer bands were excised and incubated in 200 μl of denaturing buffer (50 m*M* Tris-HCl pH 6.8, 30% glycerol, 2% SDS, 6 *M* urea,1 *M* DTT) for 30 min at 54°C. The sample was separated by reducing SDS-PAGE as the second dimension and stained with colloidal Coomassie.

Western blot analyses

For Western blot analyses, the proteins were blotted onto nitrocellulose membranes (GE Healthcare). α-YchF antibodies were raised in rabbits against the peptide VNEDGFENNPYLDQC. α-TrxA antibodies were obtained from Sigma. A horseradish peroxidase-coupled secondary antibody was used for detection; blots were incubated for 1 min with homemade enhanced chemiluminescence reagent and signals were detected by a CCD camera.

In vivo *site-directed cross-linking*

E. coli cells carrying pSUP-BpaRS-6TRN and pBad-YchFN20, pBad-YchFR146, or pBad-YchFA160 were grown overnight and used for the inoculation of 400 ml LB; 0.5 m*M* pBpA in 1 *M* NaOH was added and cells were grown at 37°C to an OD of 0.3 before they were induced by 0.001% arabinose. Cells were harvested after 3 h of growth and resuspended in 8 ml PBS buffer. Half of the sample was transferred into a six-well microtiter plate and treated with UV light (0.12 J/cm^2) (UV Transilluminator Vilber Lourmat BLX-365) for 20 min. The other half was protected against UV light. YchF was then purified from UV-exposed and control cells following the protocol described above. To analyze the effect of thiol depletion on *in vivo* cross-linking, cells were treated for 30 min with 50 μM diamide (Sigma) at 37°C before harvesting.

Protein identification and quantification by mass spectrometry

Lanes of an SDS gel of purified samples were cut into equal slices and subjected to in-gel digestion using trypsin, followed by nano-UHPLC/MS analysis essentially as described (38). The LTQ-FT-Ultra (Thermo Fisher Scientific) was operated with settings as described (33), except that survey full MS spectra were collected at a resolution of 25,000 with an automatic gain control target value of 2×10^6 ions. Proteins were identified by database searches using the MaxQuant program version 1.3.0.5 (12, 13) as described (33), selecting carbamidomethylation of cysteine as a fixed modification. Protein sequences were taken from the UniProt database (50) for *E. coli* (version 2013_07, taxonomy: 83333, keywords: 181 and 1185). Intensities per protein (representing the sum of unique peptide intensities) and per gel slice were used to generate profiles for individual gel lanes and to estimate the molecular mass of cross-link products by extrapolation. Relative quantification was done by dividing the total intensity per protein observed in the control lane (−UV) by that observed in the +UV lane.

Identification of disulfide bonds by mass spectrometry

To block free cysteine residues, purified YchF (3.5 mg) was treated with 100 m*M* iodoacetamide for 15 min at 37°C before separation by SDS-PAGE. After colloidal Coomassie staining, the monomer and the dimer bands were excised. Gel slices were washed and destained by five successive alternate 10-min incubations with 10 m*M* NH_4HCO_3, followed by 50% ethanol in 10 m*M* NH_4HCO_3. To minimize disulfide scrambling, the pH was adjusted to 6.5 with acetic acid. Furthermore, 2 m*M* N-ethylmaleimide (NEM) was included in both solutions to prevent the formation of non-native disulfide bonds. In-gel protein digestion using trypsin was carried out at pH 6.5 in 10 m*M* NH_4HCO_3 supplemented with 2 m*M* NEM. Samples were incubated with 66 ng trypsin (sequencing grade modified, Promega) per gel slice for 15 h at 37°C. Peptides were eluted in 0.05% trifluoroacetic acid (TFA)/50% acetonitrile (ACN), dried in vacuum, and redissolved in 15 μl 0.1% TFA. Samples were analyzed by nano-HPLC/ESI-MS/MS as described (33), except that peptides were separated on a 50 cm × 70 μm C18 column (Acclaim PepMap RSLC column, 2 μm particle size, 100 Å pore size; Thermo Scientific) at a flow rate of 250 nl/min with a linear gradient consisting of 1% to 65% solvent B (0.1% formic acid, 4% dimethylsulfoxide, 30% methanol, 48% ACN) for 30 min. The identification of disulfide-linked peptides is described in Supplementary Data.

Cysteine labeling with PEG-Mal

Purified YchF in 50 m*M* Tris-HCl, pH 7.5, 5 m*M* $MgCl_2$, and 200 m*M* NaCl was reduced by incubating it for 1 h at 4°C with 150 μl Thermo Scientific™ Immobilized TCEP Disulfide Reducing Gel and subsequently incubated with 0.75 m*M* PEG-MAL (in DMSO) for 15 min at 25°C. Loading buffer (–DTT) was added and the samples were denatured at 37°C for 10 min and loaded onto SDS-PAGE.

Cysteine labeling with fluorescein-5-maleimide

Purified YchF (5 mg) was reduced by incubation with TCEP Reducing Gel for 2 h at 4°C and continuous shaking (750 rpm). After centrifugation (21, 000 *g*, 3 min), ~50 μg of fluorescein-5-maleimide (in HT buffer) was added to the supernatant, followed by a 2-h incubation at room temperature. Precipitates were removed by centrifugation (21, 000 *g*, 1 min) and both supernatant and pellet were denatured for 10 min at 54°C in Laemmli loading buffer (–DTT). After SDS-PAGE, fluorescence was detected using a CCD camera.

Acknowledgments

This work was supported by grants from the Deutsche Forschungsgemeinschaft to B.W. and H.G.K., the Excellence Initiative of the German Federal and State Governments (Grant EXC 294 BIOSS Centre for Biological Signalling Studies) to B.W., the Else-Kröner-Fresenius Stiftung and the Motivate MD College of the University Freiburg Medical School to L.H., and the Chinese Scholarship Council to Q.B. The authors thank the National Institute of Genetics, Japan, for *E. coli* strains, JW1194 (Δ*ychF*) and MY1013 (Δ*trxA*).

Author Disclosure Statement

No competing financial interests exist.

References

1. Akhova AV and Tkachenko AG. ATP/ADP alteration as a sign of the oxidative stress development in *Escherichia coli* under antibiotic treatment. *FEMS Microbiol Lett* 353: 69–76, 2014.
2. Alexander RW and Schimmel P. Domain-domain communication in aminoacyl-tRNA synthetases. *Prog Nucleic Acid Res Mol Biol* 69: 317–349, 2001.
3. Antelmann H and Helmann JD. Thiol-based redox switches and gene regulation. *Antioxid Redox Signal* 14: 1049–1063, 2011.
4. Aslund F, Zheng M, Beckwith J, and Storz G. Regulation of the OxyR transcription factor by hydrogen peroxide and the cellular thiol-disulfide status. *Proc Natl Acad Sci U S A* 96: 6161–6165, 1999.
5. Baker LM and Poole LB. Catalytic mechanism of thiol peroxidase from *Escherichia coli*. Sulfenic acid formation and overoxidation of essential CYS61. *J Biol Chem* 278: 9203–9211, 2003.
6. Becker M, Gzyl KE, Altamirano AM, Vuong A, Urban K, and Wieden HJ. The 70S ribosome modulates the ATPase activity of *Escherichia coli* YchF. *RNA Biol* 9: 1288–1301, 2012.
7. Charles R, Jayawardhana T, and Eaton P. Gel-based methods in redox proteomics. *Biochim Biophys Acta* 1840: 830–837, 2014.
8. Chen YC and Chung YT. A conserved GTPase YchF of Vibrio vulnificus is involved in macrophage cytotoxicity, iron acquisition, and mouse virulence. *Int J Med Microbiol* 301: 469–474, 2011.
9. Cheung MY, Li MW, Yung YL, Wen CQ, and Lam HM. The unconventional P-loop NTPase OsYchF1 and its regulator OsGAP1 play opposite roles in salinity stress tolerance. *Plant Cell Environ* 36: 2008–2020, 2013.
10. Cheung MY, Xue Y, Zhou L, Li MW, Sun SS, and Lam HM. An ancient P-loop GTPase in rice is regulated by a higher plant-specific regulatory protein. *J Biol Chem* 285: 37359–37369, 2010.
11. Choi H, Kim S, Mukhopadhyay P, Cho S, Woo J, Storz G, and Ryu SE. Structural basis of the redox switch in the OxyR transcription factor. *Cell* 105: 103–113, 2001.
12. Cox J and Mann M. MaxQuant enables high peptide identification rates, individualized p.p.b.-range mass accuracies and proteome-wide protein quantification. *Nat Biotechnol* 26: 1367–1372, 2008.
13. Cox J, Neuhauser N, Michalski A, Scheltema RA, Olsen JV, and Mann M. Andromeda: a peptide search engine integrated into the MaxQuant environment. *J Proteome Res* 10: 1794–1805, 2011.
14. Croze E, Yamaguchi KD, Knappertz V, Reder AT, and Salamon H. Interferon-beta-1b-induced short- and long-term signatures of treatment activity in multiple sclerosis. *Pharmacogenomics J* 13: 443–451, 2013.
15. Danese I, Haine V, Delrue RM, Tibor A, Lestrate P, Stevaux O, Mertens P, Paquet JY, Godfroid J, De Bolle X, and Letesson JJ. The Ton system, an ABC transporter, and a universally conserved GTPase are involved in iron utilization by Brucella melitensis 16M. *Infect Immun* 72: 5783–5790, 2004.
16. Gradia DF, Rau K, Umaki AC, de Souza FS, Probst CM, Correa A, Holetz FB, Avila AR, Krieger MA, Goldenberg S, and Fragoso SP. Characterization of a novel Obg-like ATPase in the protozoan *Trypanosoma cruzi*. *Int J Parasitol* 39: 49–58, 2009.
17. Haghdoost S, Sjölander L, Czene S, Harms-Ringdahl M. The nucleotide pool is a signficant target for oxidative stress. *Free Radic Biol Med* 41: 620–626, 2006.
18. Hoffmann JH, Linke K, Graf PC, Lilie H, and Jacob U. Identification of a redox-regulated chaperone network. *Embo J* 23: 160–168, 2004.
19. Imlay JA. Cellular defenses against superoxide and hydrogen peroxide. *Annu Rev Biochem* 77: 755–776, 2008.
20. Imlay JA. The molecular mechanisms and physiological consequences of oxidative stress: lessons from a model bacterium. *Nat Rev Microbiol* 11: 443–454, 2013.
21. Jacob KD, Noren-Hooten N, Trzeciak AR, and Evans MK. Marker of oxidant stress that are clinically relevant in aging and age-related disease. *Mech Ageing Dev* 134: 139–157, 2013.
22. Jeyabal PV, Rubio V, Chen H, Zhang J, and Shi ZZ. Regulation of cell-matrix adhesion by OLA1, the Obg-like ATPase 1. *Biochem Biophys Res Commun* 444: 568–574, 2014.
23. Kira Y and Nishikawa M. The identification and characterization of a new GTP binding protein (Gbp45) involved in cell proliferation and death related to mitochondrial function. *Cell Mol Biol Lett* 13: 570–584, 2007.
24. Koller-Eichhorn R, Marquardt T, Gail R, Wittinghofer A, Kostrewa D, Kutay U, and Kambach C. Human OLA1 defines an ATPase subfamily in the Obg family of GTP-binding proteins. *J Biol Chem* 282: 19928–19937, 2007.

25. Kuhn P, Weiche B, Sturm L, Sommer E, Drepper F, Warscheid B, Sourjik V, and Koch HG. The bacterial SRP receptor, SecA and the ribosome use overlapping binding sites on the SecY translocon. *Traffic* 12: 563–578, 2011.
26. Lee JW and Helmann JD. The PerR transcription factor senses H2O2 by metal-catalysed histidine oxidation. *Nature* 440: 363–367, 2006.
27. Lu J and Holmgren A. The thioredoxin antioxidant system. *Free Radic Biol Med* 66: 75–87, 2014.
28. Macek B, Gnad F, Soufi B, Kumar C, Olsen JV, Mijakovic I, and Mann M. Phosphoproteome analysis of *E. coli* reveals evolutionary conservation of bacterial Ser/Thr/Tyr phosphorylation. *Mol Cell Proteomics* 7: 299–307, 2008.
29. Matsuzuwa A, Kanno S-i, Nakayama M, Mochiduki H, Wei L, Shimaoka T, Furukuwa Y, Kato K, Shibata S, Ishioka C, and Chiba N. The BRCA1/BRAD1-interacting protein Ola1 functions in centrosome Regulation. *Mol Cell* 53: 101–114, 2014.
30. Miller E, Wachnowicz B, and Majsterek I. Advances in oxidative therapy of multiple sclerosis. *Curr Med Chem* 20: 4720–4730, 2013.
31. Mori H and Ito K. Different modes of SecY-SecA interactions revealed by site-directed *in vivo* photo-cross-linking. *Proc Natl Acad Sci U S A* 103: 16159–16164, 2006.
32. Nabilsi NH, Broaddus RR, and Loose DS. DNA methylation inhibits p53-mediated survivin repression. *Oncogene* 28: 2046–2050, 2009.
33. Niemann M, Wiese S, Mani J, Chanfon A, Jackson C, Meisinger C, Warscheid B, and Schneider A. Mitochondrial outer membrane proteome of trypanosoma brucei reveals novel factors required to maintain mitochondrial morphology. *Mol Cell Proteomics* 12: 515–528, 2013.
34. Nishiyama A, Matsui K, Iwata S, Hirota K, Masutani H, Nakamura H, Takagi Y, Sono H, Gon Y, and Yodoi J. Identification of thioredoxin-binding protein-2/vitamin D(3) up-regulated protein 1 as a negative regulator of thioredoxin function and expression. *J Biol Chem* 274: 21645–21650, 1999.
35. Parry DAD, Fraser RDB, and Squire JM. Fifty years of coiled-coils and α-helical bundles: A close relationship between sequence and structure. *J Struct Biol* 163: 258–269, 2008.
36. Putnam CD, Arvai AS, Bourne Y, and Tainer JA. Active and inhibited catalase structures: ligand and NADPH binding and catalytic mechanism. *J Mol Biol* 296: 295–309, 2000.
37. Ryu Y and Schultz PG. Efficient incorporation of unnatural amino acids into proteins in *Escherichia coli*. *Nat Methods* 3: 263–265, 2006.
38. Sachelaru I, Petriman NA, Kudva R, Kuhn P, Welte T, Knapp B, Drepper F, Warscheid B, and Koch HG. YidC occupies the lateral gate of the SecYEG translocon and is sequentially displaced by a nascent membrane protein. *J Biol Chem* 288: 16295–16307, 2013.
39. Samanfar B, Tan le H, Shostak K, Chalabian F, Wu Z, Alamgir M, Sunba N, Burnside D, Omidi K, Hooshyar M, Galvan Marquez I, Jessulat M, Smith ML, Babu M, Azizi A, and Golshani A. A global investigation of gene deletion strains that affect premature stop codon bypass in yeast, Saccharomyces cerevisiae. *Mol Biosyst* 10: 916–924, 2014.
40. Scott TL, Rangaswamy S, Wicker CA, and Izumi T. Repair of oxidative DNA damage and cancer: recent progress in DNA base excision repair. *Antioxid Redox Signal* 20: 708–726, 2014.
41. Seaver LC and Imlay JA. Are respiratory enzymes the primary sources of intracellular hydrogen peroxide? *J Biol Chem* 279: 48742–48750, 2004.
42. Shutt T, Geoffrion M, Milne R, and McBride HM. The intracellular redox state is a core determinant of mitochnodrial fusion. *EMBO Rep* 13: 909–915, 2012.
43. Sinha K, Das J, Pal PB, and Sil PC. Oxidative stress: the mitochondria-dependent and mitochondria-independent pathway of apoptosis. *Arch Toxicol* 87: 1157–1580, 2013.
44. Song H, Cha MJ, Song BW, Kim IK, Chang W, Lim S, Choi EJ, Ham O, Lee SY, Chung N, Jang Y, and Hwang KC. Reactive oxygen species inhibit adheasion of mesenchymal stemm cells implanted into ischemic myocardium via interference of focal adheasion complex. *Stem Cells* 31: 555–563, 2010.
45. Stebbins CE, Borukhov S, Orlova A, Polyakov A, Goldfarb A, and Darst SA. Crystal structure of the GreA transcript cleavage factor from *Escherichia coli*. *Nature* 373: 636–640, 1995.
46. Sun H, Luo X, Montalbano J, Jin W, Shi J, Sheikh MS, and Huang Y. DOC45, a novel DNA damage-regulated nucleocytoplasmic ATPase that is overexpressed in multiple human malignancies. *Mol Cancer Res* 8: 57–66, 2010.
47. Teplyakov A, Obmolova G, Chu SY, Toedt J, Eisenstein E, Howard AJ, and Gilliland GL. Crystal structure of the YchF protein reveals binding sites for GTP and nucleic acid. *J Bacteriol* 185: 4031–4037, 2003.
48. Thapa B and Schlegel HB. Calculations of pKa's and redox potentials of nucelobases with explicit waters and polarizable continuum solvation. *J Phys Chem* 119: 5134–5144, 2015.
49. Tomar SK, Kumar P, and Prakash B. Deciphering the catalytic machinery in a universally conserved ribosome binding ATPase YchF. *Biochem Biophys Res Commun* 408: 459–464, 2011.
50. UniProtConsortium. Activities at the Universal Protein Resource (UniProt). *Nucleic Acids Res* 42: D191, 2013.
51. Veal EA, Day AM, and Morgan BA. Hydrogen peroxide sensing and signaling. *Mol Cell* 26: 1–14, 2007.
52. Verstraeten N, Fauvert M, Versees W, and Michiels J. The universally conserved prokaryotic GTPases. *Microbiol Mol Biol Rev* 75: 507–542, 2011.
53. Wenk M, Ba Q, Erichsen V, MacInnes K, Wiese H, Warscheid B, and Koch HG. A universally conserved ATPase regulates the oxidative stress response in *Escherichia coli*. *J Biol Chem* 287: 43585–43598, 2012.
54. Wittinghofer A and Vetter IR. Structure-function relationsships of the G-domain, a canonical switch motif. *Ann Rev Biochem* 80: 943–971, 2011.
55. Yoshikara E, Masaki S, Matsuo Y, Chen Z, Tian HF, and Yodoi J. Thioredoxin/Txnip: redoxisome, as a redox switch for the pathogenesis of diseases. *Front Immunol* 4: 514, 2014.
56. Zhang J, Rubio V, Lieberman MW, and Shi ZZ. OLA1, an Obg-like ATPase, suppresses antioxidant response via nontranscriptional mechanisms. *Proc Natl Acad Sci U S A* 106: 15356–15361, 2009.
57. Zhang JW, Rubio V, Zheng S, and Shi ZZ. Knockdown of OLA1, a regulator of oxidative stress response, inhibits motility and invasion of breast cancer cells. *J Zhejiang Univ Sci B* 10: 796–804, 2009.

58. Zheng M, Aslund F, and Storz G. Activation of the OxyR transcription factor by reversible disulfide bond formation. *Science* 279: 1718–1721, 1998.
59. Zheng M, Wang X, Doan B, Lewis KA, Schneider TD, and Storz G. Computation-directed identification of OxyR DNA binding sites in *Escherichia coli*. *J Bacteriol* 183: 4571–4579, 2001.
60. Zheng M, Wang X, Templeton LJ, Smulski DR, LaRossa RA, and Storz G. DNA microarray-mediated transcriptional profiling of the *Escherichia coli* response to hydrogen peroxide. *J Bacteriol* 183: 4562–4570, 2001.

Address correspondence to:
Prof. Hans-Georg Koch
Institut für Biochemie und Molekularbiologie
Albert-Ludwigs-Universität Freiburg
Stefan-Meier Strasse 17
Freiburg 79104
Germany

E-mail: hans-georg.koch@biochemie.uni-freiburg.de

Date of first submission to ARS Central, January 28, 2015; date of final revised submission, June 22, 2015; date of acceptance, July 9, 2015.

Abbreviations Used

BRCA1 = breast cancer-associated gene 1
DTT = dithiothreitol
EDTA = ethylenediaminetetraacetic acid
FDR = false discovery rate
IPTG = isopropyl β-D-1-thiogalactopyranoside
Obg = spo0B-associated GTP-binding protein
OD = optical density
pBpa = para-benzoyl-L-phenylalanin
PBS = phosphate-buffered saline
PEG-Mal = methoxypolyethylene glycol maleimide
PMSF = phenylmethylsulfonyl fluoride
SDS-PAGE = sodium dodecyl sulfate–polyacrylamide gel electrophoresis
TCEP = tris(2-carboxyethyl)phosphine
TGS-domain = ThrRS-GTPases-SpoT
TRAFAC = translation factor